KSCE Journal of Civil Engineering (2020) 24(6):1696-1705
DOI 10.1007/s12205-020-0574-4

pISSN 1226-7988, eISSN 1976-3808
www.springer.com/12205

Geotechnical Engineering

Failure Mechanism of a Granular Bed Induced by a Horizontal Water Jet Using Particle Image Velocimetry

Majed Omar Alsaydalani[a]

[a]*Civil Engineering Department, Umm Al-Qura University, Makkah 21955, Saudi Arabia*

ARTICLE HISTORY

Received 2 April 2019
Revised 15 September 2019
Accepted 13 January 2020
Published Online 1 May 2020

KEYWORDS

Particle image velocimetry
Failure mechanism
Local fluidisation
Horizontal flow
Seepage

ABSTRACT

Particle image velocimetry (*PIV*) was used to investigate the failure mechanism of a granular bed subjected to a water jet emerging laterally from a vertical, impermeable face. Experiments were performed in a modified seepage tank made of plexiglass with dimensions of 700 × 600 × 103 mm. The bed of particles was subjected to a lateral seepage flow at a controlled rate, and the motion of the particles was recorded using a digital camera. Measurements of flow and pore pressure were also made. Several stages of failure were observed during the repeated experiments: 1) outwards movement of the particles (horizontally and vertically upwards), 2) cavity formation, 3) cavity enlargement, and 4) the emergence of a fluidised zone at the bed surface. Trends relating to the flow rate of fluid flow to the onset of failure were also noted. The *PIV* analyses revealed the movement of sand grains and boundaries between regions in which sand grains either did or did not move. An analytical model based on the Ergun equation is presented to predict the onset of failure. This study provides valuable insights into the failure mechanism of granular materials triggered by lateral seepage flow.

1. Introduction

Failure by seepage flow is considered to cause some of the most serious accidents in civil engineering. Such failure can occur in a number of situations in which there is a source for uncontrolled or poorly controlled seepage flow. For example, it may occur through dam cores (Kjaernsli and Torblaa, 1968; Richards and Reddy, 2007; Omofunmi et al., 2017), seepage barriers (e.g., Rice and Duncan, 2010), suction caissons (Allersma et al., 2003; Tran et al., 2004; Harireche et al., 2014) and fractured underground broken water pipes (Al-Karni, 2000; Walski et al., 2006; van Zyl and Clayton, 2007; van Zyl et al., 2013).

The tragic failure of Teton Dam in the United States in 1976 resulted in the deaths of 11 people and caused over $1 billion in property damages. Various failure mechanics have been suggested as being responsible for the failure of this dam, including internal erosion and the formation of a hydraulic fracture in the core of the dam (Pillai et al., 2004). Unfortunately, when a structure fails due to localised flow, the evidence is often washed away with the structure.

Traditionally, failure by seepage flow is perceived as resulting from piping phenomena in which erosion of the structure starts at the exit point of seepage; progressive backward erosion along its base leading to the formation of a continuous passage or pipe (Terzaghi, 1939). Darcy flow initiates piping at the exit point where the flow is laminar. However, failures by seepage flow are complex and may involve other mechanisms, particularly when the seepage flow does not adhere to Darcy's law (e.g., in the case of flow through defects).

There is a considerable amount of literature related to failure by seepage flow (for example, see Richards and Reddy, 2007; Omofunmi et al., 2017) and these are mainly based on soil seepage analysis, where Darcy's law is generally applied. Darcy's law assumes laminar flow, which suggests that the rate of flow, and thus velocity, is linearly proportional to the hydraulic head and inversely proportional to the length of the flow path. Laminar flow could occur at low rates; at higher rates, such as those occurring in the vicinity of the defect, are more complex (Niven, 2002). The critical value of Re (Re = V D/ν, where V is the average velocity of flow (flow per unit cross section of soil), D is the average diameter of soil particles and ν is the fluid kinematic viscosity) at which flow in soil changes from laminar to turbulent has been found to range between about 1 and 10 (e.g., Harr, 1962). Niven (2002) noted that the deviation from laminar flow

CORRESPONDENCE Majed Omar Alsaydalani ✉ mosaydalani@uqu.edu.sa Civil Engineering Department, Umm Al-Qura University, Makkah 21955, Saudi Arabia

occurs at a value of Re ~ 5.

Further, flow through defects in a structure into the surrounding soil is unlikely to adhere to Darcy's law, because of the interaction of soil particles with the defect, turbulent flow in the soil and the changing geometry of the unconfined flow regime (van Zyl and Clayton, 2007; Alsaydalani and Clayton, 2014). The size of defect and the distribution of internal stresses may play a critical role in the failure mechanism.

An understanding of the failure mechanisms induced by seepage flow is important from both a practical and a theoretical perspective. Recently, He et al. (2017) studied the behaviour of a granular bed subjected to an upward-facing water jet using an experimental model simulating a defected water pipe. These authors observed that different stages are associated with the flow rate that appeared to outline the bed's behaviour: no cavity, a stable cavity above the jet, unstable cavity and full fluidisation. He et al. (2017) proposed an analytical model based on force equilibrium and Darcy's law to predict the critical rate of flow for fluidisation.

Alsaydalani and Clayton (2014) conducted a series of physical experiments exploring and explaining the behaviour of granular materials during fluidisation using a two-dimensional experimental model with a vertical water jet. These authors controlled the rate of flow in their tests, incrementally increasing it until internal fluidisation was initiated. At this point, the upward vertical force exerted by the seepage flow exceeded the weight of the granular bed in the active area of flow, which took on the shape of a wedge above the source of the flow. Alsaydalani and Clayton (2014) found that increasing the rate of flow at an orifice (e.g., a defective pipe) into a granular bed initially led to the build-up of pore water pressure and an increase in hydraulic gradients in the vicinity of the opening, where Darcy's flow can be expected; an increase in the rate of flow resulted in non-Darcy flow. Alsaydalani and Clayton (2014) noted that internal fluidisation phenomena might occur in many unseen situations, with effects similar to the piping phenomenon, as a result of the loss of stability of the granular matter in which it occurs.

Simulating water flow from buried pipes, van Zyl et al. (2013) conducted an experimental study of soil fluidisation using upward-pointing jets. These authors performed tests at controlled flow rates and observed the behaviour of the bedding material. van Zyl et al. (2013) noted that as soon as the water jet was introduced into the bed of granular material, fluidised zones developed and grew rapidly at the bottom of the bed until they reached a stable state. Once this state was reached, the geometries of the zones remained constant, apart from the minor fluctuations of the terminating head of the fluidised zone. One important observation of this study was that some pressure can be maintained in a leaking underground pipe without observing a fluidised zone at the bed surface.

Zoueshtiagh and Merlen (2007) adopted an experimental approach to studying the behaviour of a granular bed subjected to a vertically directed jet of water. Using a three-dimensional experimental model, these authors showed that, depending on the rate of flow, three different regimes characterise the behaviour of the bed: i) a stable bed at a sufficiently low flow rate, ii) a deformed bed (a transitional regime) in which the bed top surface is deformed and iii) a fluidised bed in which the bed explodes and fluidisation at the bed surface is observed. Zoueshtiagh and Merlen's (2007) observations of regime ii) suggest a high potential for the occurrence of internal mechanisms at the orifice-particle interface. However, limitations in experimental design (i.e., the problem was studied in three dimensions), did not allow them to observe such mechanisms. These authors postulated that observations of this regime could be linked with arch formation near the source of the flow.

Using particle image velocimetry (*PIV*), Tran et al. (2005) studied the mechanism of sand heave formed in suction caissons. They developed an apparatus with a half-caisson model and carried out experiments in dense silica sand with different caisson wall penetration depths. A high-resolution camera was used to capture sand movement and was subsequently analysed using *PIV* to identify the different zone of sand movement. The results showed two distinct areas of sand movement: a large displacement zone in the two regions close to the inner caisson wall, while the remaining field showed no movement. The largest observed displacement was adjacent to the inner wall and resembled a wedge shape. Tran et al. (2005) noted that the majority of sand heave observed was a result of dilation of the sand plug rather than sand inflow.

Niven and Khalili (1998) conducted an experiment on the scouring of granular material by an internal, downwardly directed, vertical water jet. These authors conducted a series of experiments using different granular materials and jet diameters and plexiglass tanks of different sizes. In some of these experiments, the jet was positioned near the tank wall to visualise the scour zone. This set-up yielded a localised, fluidised region that changed shape as the jet depth increased which then produced a submerged fluidised cavity. Niven and Khalili (1998) observed that for any given material, jet diameter and rate of flow, the fluidised zone profile remained nearly constant in shape. They also observed that the geometry of the fluidised zone was controlled by two mechanisms: i) scour at the point source of flow and ii) the fluid flow's ability to sustain fluidisation, which controls the zone diameter.

These results testify to the substantial efforts exerted by researchers to explain and investigate the behaviour of granular materials subjected to seepage flow in which the bedding material was subjected to vertical seepage flow (either using a vertically upward-directed water jet or a downward-directed vertical water jet). However, it is expected that if the water is injected horizontally, although it flows predominantly vertically, it plays a critical role in the failure mechanism and geometry of deformation.

This paper presents the results of a series of experiments conducted to investigate and monitor the behaviour of a granular bed subjected to lateral seepage flow as a simple model of a defect in an earth dam or a sheet-pile retaining wall. The experiments were performed in modified seepage tanks with a two-dimensional flow of water into saturated granular sand. Measurements of

flow and pressure were obtained, and the *PIV* technique was used to monitor the behaviour of the granular bed.

2. Experimental Set-Up

Figure 1 displays a schematic diagram of the experimental apparatus, which contained a defect that allowed for the formation of lateral seepage flow. The experimental apparatus consisted of a seepage tank made of steel frame and clear plexiglass that enabled observations of the behaviour of the bed; the tank dimensions were 700 × 600 × 103 mm. The pump was manufactured by Armfield (England) and the rest of the set-up included a water storage tank, pipes to connect the pump to seepage tank, valves to control flow rate and a Sony digital video camera (HDR-SR11; Sony Corporation, Japan).

2.1 Monitoring the Behaviour of the Granular Bed Using Particle Image Velocimetry

Thanks to its advantages over other methods, the *PIV* technique was adopted in this study to monitor the behaviour of the granular bed. For example, *PIV* is a non-intrusive technique (Adrian, 1991) increasingly employed in a variety of disciplines. It has been widely used to study the behaviour of granular beds and the movement of particles in beds.

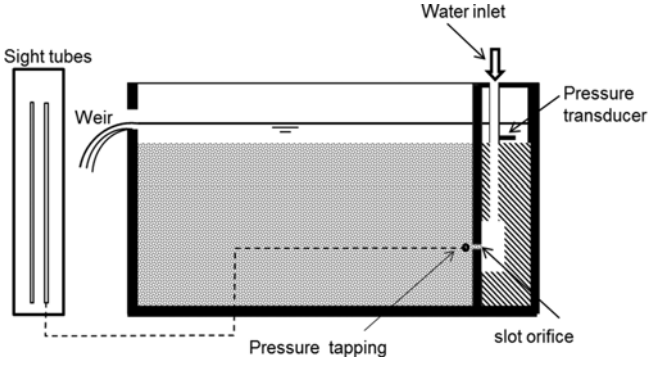

Fig. 1. Schematic Diagram of the Experimental Apparatus for lAteral Flow

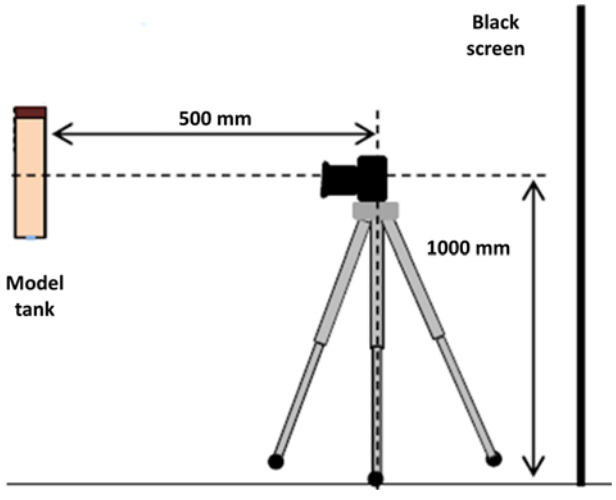

Fig. 2. Sketch of the Experimental Set-Up for *PIV*

The *PIV* set-up is shown schematically in Fig. 2. The set-up consists of a light source, a camera, a board with gridlines and image processing software to track the movement of the particles.

The behaviour of the bed was examined using a video camera with a resolution of 1,920 × 1,080 pixels operating at 25 frames per second. The camera was positioned at a distance of 500 mm from the clear plexiglass wall of the tank, affording a view measuring 600 mm × 400 mm, which was sufficiently large to encompass the specimens prepared for the experiments. During each experiment, video recordings of the behaviour of the granular bed were obtained. These recordings were then analysed and converted to frames using image processing software. Once the images of the interested zone were selected, they were analysed using the *PIV* technique. MatPIV code written in MATLAB by Sveen (2004) was used in this study. A signal-to-noise ratio (s/n) filter with a ratio of 1.3 (as suggested by Keane and Adrian, 1992) and global and local mean filters were applied to remove the outlier vectors of the resulting data.

2.2 Measurements of the Flow Rate through the Defect

Measurements of the flow rate through the defect were obtained using a flow meter (Georg Fischer *LLC*, United States; model Signet 2551) with an *LCD* display unit. According to the flow meter's specifications, it achieves ± 2% accuracy and has an operating range of up to 18.23 m³/h for a 1 in pipe diameter. The meter has a function for averaging flow rate (i.e., setting a time over which the meter averages the flow signals). During the experimental run, this function was adjusted to 30 seconds to help smooth the display on the *LCD*.

2.3 Measurements of Excess Pore Pressure

Measurements of excess pore water pressure within the granular sand were obtained using a standpipe. A hole 2 mm in diameter was drilled through the back wall of the tank. This hole was aligned with the defect and made 10 mm away from it. A syringe with an internal diameter of 1 mm was introduced through this hole. This syringe was long enough (about 50 mm on each side) to provide a suitable point of connection for the standpipe and to reach the centre line of the tank. Before preparing the test sample in the tank, the needle inside it was covered with a screen (i.e., filter) to prevent grains from entering the syringe, thus avoiding blocking the syringe, which might otherwise affect the measured pressure in the bed. Pore water pressure measurements were read directly from a vertically positioned water manometer, providing an accuracy of ± 1 mm of the water column.

2.4 Materials Tested and Specimen Preparation

The tests were carried out using silica sand as bed material. An electron micrograph of this material is shown in Fig. 3; the sand is sub-rounded and slightly elongated and flattened. The particle-size distribution of silica sand is shown in Fig. 4; it ranged from 0.6 to 1.18 mm, with a D50 size of 0.9 mm.

Soil specimens were prepared by pouring a known weight of

Fig. 3. Scanning Electron Micrographs of the Tested Material (silica sand)

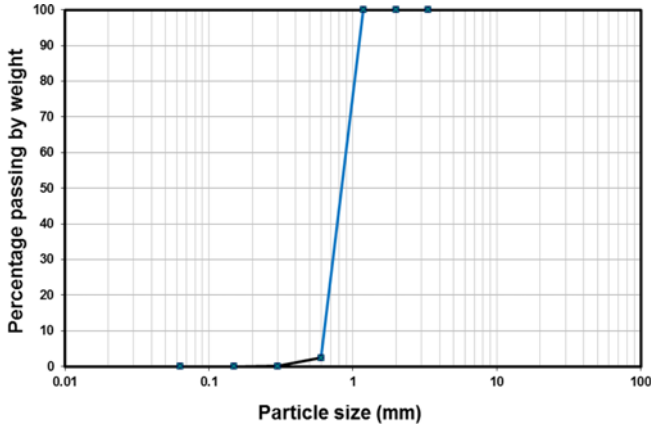

Fig. 4. Particle-Size Distribution of the Tested Material

dry sand from a funnel with a 16 mm-diameter nozzle into the tank. The height of the pouring was kept constant at roughly 15 mm above the water level in the tank. After deposition, specimens were densified by tapping the base of the tank in a symmetrical pattern using a rammer. Table 1 lists the dry density, specific gravity, void ratio and relative density of the specimen. The permeability coefficient of the tested material was measured in the lab using the constant head method to be 0.32 cm/s.

2.5 Test Procedure

The tests were carried out under controlled flow rates while the behaviour of the granular bed was monitored. Water was allowed to flow horizontally through the defect into the bed of granular material. At the beginning of the test, a relatively small flow rate was applied (i.e., 75 l/h), which was then increased incrementally until failure of the granular bed occurred and the cavity broke through to the bed surface. For each flow rate, the pore pressure in the granular bed was recorded after being allowed to stabilise (for about 2 minutes). Pore water pressure was measured using a water manometer, and the flow rates were recorded directly from the flow meter. A video camera was used to monitor the behaviour of the bed as the flow rate developed. The generated videos were then analysed and converted into pictures (i.e., images) and subsequently analysed using the *PIV* technique to detect any changes in the bed behaviour (see Section 2.1 for details). Vectors were then generated using *PIV* to represent the displacement and direction of sand movement at the start of the failure mechanism and in other cases at developing flow rates. The observations obtained using *PIV*, coupled with data obtained from the flow meter and the manometer, helped to distinguish the different phases of the failure mechanism.

3. Results and Discussion

3.1 Failure Mechanism Phases

Several stages of failure were observed during the experiments. The failure mechanisms observed included 1) outwards movement of the particles (horizontally and vertically upwards) in the active area of flow, 2) cavity formation, 3) cavity enlargement, and 4) the emergence of a fluidised zone at the bed surface.

Figure 5 shows typical images and line drawings of the behaviour of the granular bed subjected to a horizontally facing water jet emerging from a vertical impermeable face (i.e., a simple model of a defect in an earth dam or a sheet wall pile). The vectors generated in Fig. 5 show the direction of sand movement at developing flow rates. The line drawings in Figs. 5(c) to 5(e) show the size of cavity developed at the defect with the developing flow rate. Various stages of failure can be observed in these images and drawings:

1. Initially, at low flow rates (up to 300 l/s), the particles of sand were in static equilibrium (Fig. 5(a)). The particles remained static, even at the point of injection. At this stage, the defect (i.e., opening) was partly blocked by the grains of sand.
2. As the flow rate was further increased to higher values (e.g., 374 l/s), it disturbed the static equilibrium condition of the particles in front of and above the defect (Fig. 5(b)). *PIV* analysis (Fig. 6) showed clearly that the particles were forced outward (horizontally and vertically upwards) in the active area of flow. This is the point at which the upward vertical seepage force overcame the sum of the grains' buoyant weights in the active area of flow. The pump shape deformation observed at the bed surface at this stage (Fig. 5(b)) associated with cavity formation in the vicinity of the defect (i.e., the defect-soil interface). Such a situation

Table 1. Dry Density, Specific Gravity and Relative Density Values for the Test Specimen

Material	Dry density (Mg/m^3)	Specific gravity	Void ratio	Minimum void ratio	Maximum void ratio	Relative density (%)
Silica sand (SS)	1.73	2.66	0.54	0.51	0.81	88

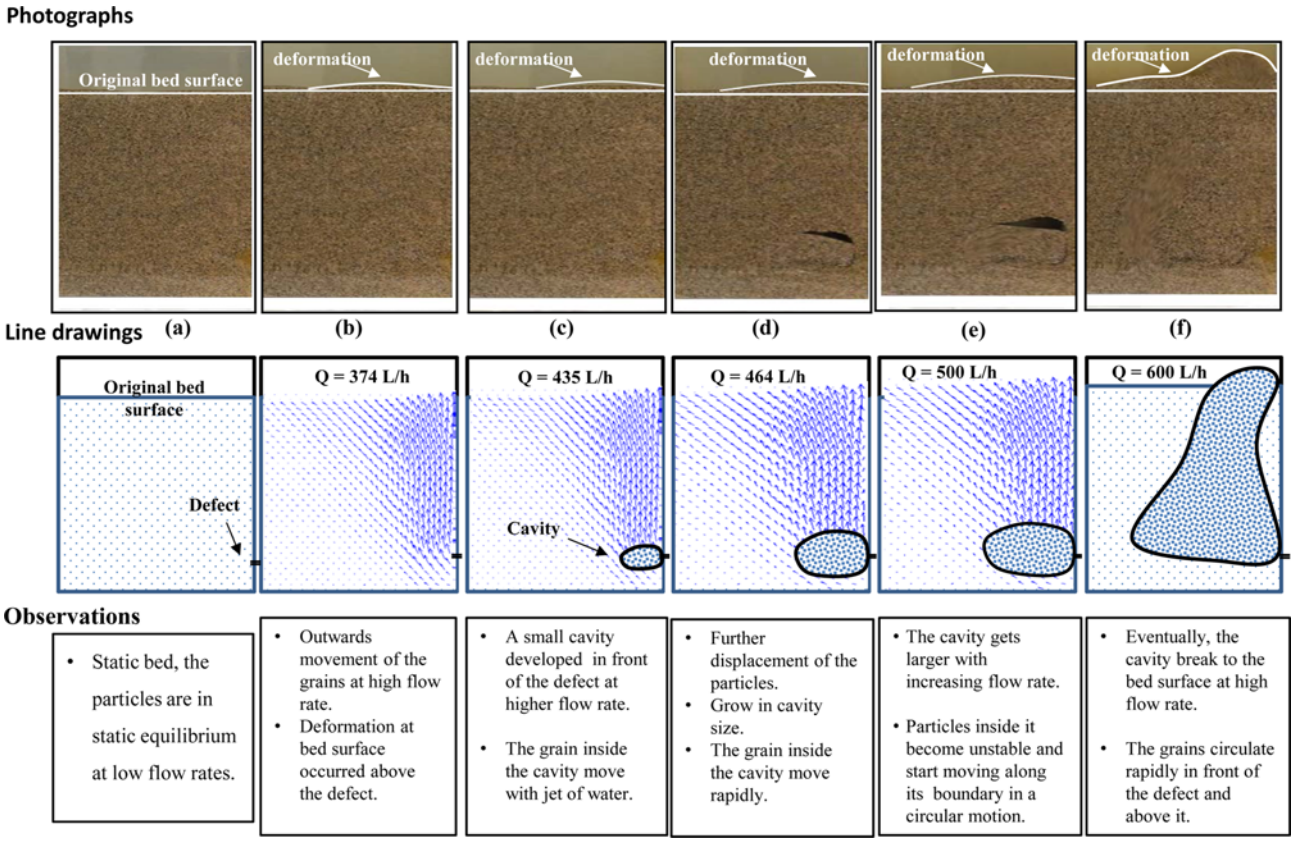

Fig. 5. Various Stages of the Failure Mechanisms of Granular Beds Induced by Lateral Flow: (a) Static Bed, (b) Outwards Movement of the Grains, (c) Cavity Formation, (d) and (e) Cavity Expansion, (f) Cavity Breaking through to the Bed Surface (bed height 200 mm, and defect opening 0.23 mm)

has been reported in the literature; for example, in the case of a granular bed lying on a tapered bed (Peng and Fan, 1997) and a vertical water jet on a granular bed (Zoueshtiagh and Merlen, 2007).

3. Following the outward movement, a small cavity was formed in front of the defect (Fig. 5(c)). The cavity here is defined as a space or hole inside the bedding material formed by a jet of water, where the grains inside it moved with the jet and those outside it remained fixed in the bed. Vectors inside the cavity were not generated because of difficulty in tracking grain movement inside the cavity. This requires a high-speed camera (higher in speed than the camera used in this experimental set-up, which operated at 25 frames per second).
4. As flow rate was further increased, the particles above the defect were displaced and the cavity size enlarged (Figs. 5(d) and 5(e)). The cavity began to expand vertically upwards and horizontally into the sample. The grains inside the cavity moved rapidly and circulated within the void. The particles became unstable and started moving along the void boundary in a circular motion resembling an elliptical shape.
5. The cavity propagated in size with the increasing flow rate; this coincided with the upward displacement of the particles above the defect. Deformation at the bed surface is shown in Fig. 5; photographs (3) to (4) demonstrate how the bed height expanded with the evolving cavity to accommodate the volume increase of the cavity.
6. As the flow increased, the cavity broke through to the bed surface forming a local fluidised bed where the grains circulated rapidly in front of the defect and above it. Fig. 5(f) shows this phase, which appears to be a large body of fluidised sand reaching the bed surface, which is not the same as a cavity.

PIV analysis (see Fig. 6) revealed that the failure mechanism of the granular bed induced by a horizontal water jet was initiated with the displacement of the grains in the active area of flow (i.e., above the defect). Fig. 6(a) gives an example with contours of the outward movement above the defect in a 350 mm-high bed with a 0.23 mm defect. The measured outward movement at the onset of failure, obtained using *PIV*, was between 1 and 10 mm. Fig. 6(b) shows the direction of sand movement at the onset of the failure, showing that particles were forced outwards (horizontally and vertically upwards) above the opening of the defect. For the horizontal-pointing defect, a right-triangular prism of material moved on the surface at 63° to the horizontal; this angle did not seem to be significantly influenced by height of the bed or width of the orifice. Following the outward displacement of sand in the bed, a cavity formed in front

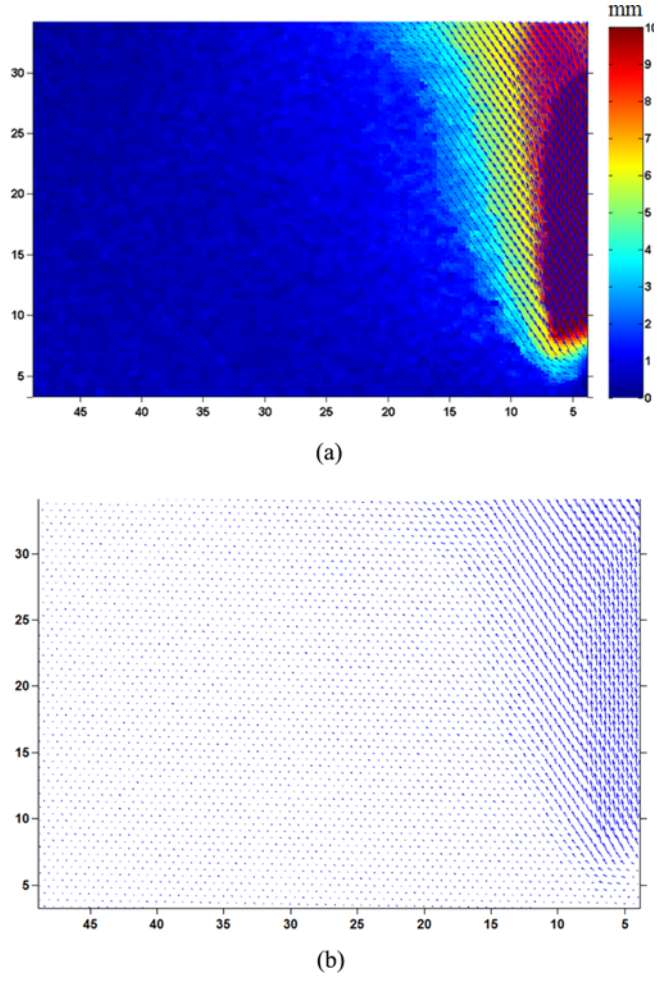

Fig. 6. *PIV* Analyses Reveal that Particles were Forced Outwards (horizontally and vertically upwards) above the Opening of the Defect: (a) Outward Movement above the Defect in a 350 mm-high bed with 0.23 mm Defect Obtained Using *PIV,* (b) Vectors Showing the Outward Movement of the Grains above the Defect in a 350 mm-high Bed with 0.23 mm Defect Obtained Using *PIV*

of the opening of the defect (see Fig. 5), which then propagated (horizontally and vertically) with the increasing flow rate. It then worked its way upward until eventually breaking through to the bed surface at a high flow rate, forming a large body of fluidised sand.

3.2 Excess Pore Water Pressure

Figure 7 shows an example of the excess pore water pressure in the bed as a function of flow rates measured at the defect for a 200 mm-thick bed of silica sand through a 0.23 mm defect opening. As the flow rate through the defect increased, the excess pore pressure in the bed increased as well (from O to A) and reached a peak at 3.54 kPa, corresponding to a rate of flow of 343 l/h. After this point, the static equilibrium of the bed was disturbed. The particles were forced outwards (horizontally and vertically upwards). This disruption was observed with the aid of *PIV* (see Fig. 6) and occurred at a flow rate of 374 l/h. The pore

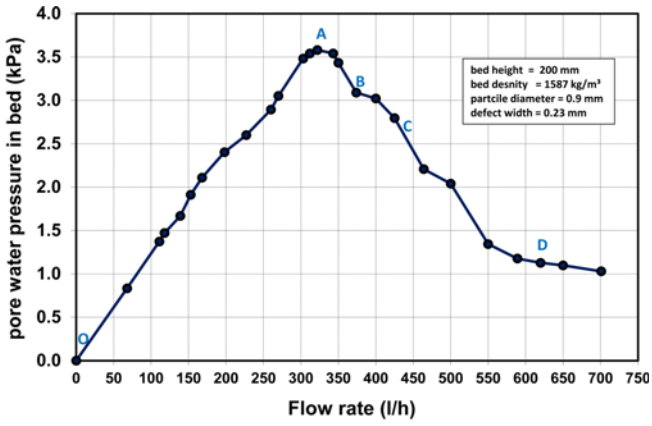

Fig. 7. Excess Pore Water Pressure in Bed with Increasing Flow Rate through the Defect in 200 mm-high Bed with 0.23 mm Defect

water pressure at this stage dropped to 3.09 kPa (point B in Fig. 7). This observed behaviour can be attributed to the state of the onset of failure at which the particles displaced outward, the bed expanded and, hence, the resistance to flow dropped. Particles displacement in the active area of flow created a space for the particles to form a cavity in the immediate vicinity of the defect. The cavity was initially observed at a flow rate of 435 l/h and a pore pressure of 2.79 kPa (point C in Fig. 7). The particles on the inside of the cavity were loosened by the jet and moved rapidly. As the flow rate was increased further, the fluidised cavity enlarged and eventually broke through to the bed surface at a flow rate of 600 l/h. At that point, the pore water pressure dropped to about 1 kPa (point D in Fig. 7). Experimental observations suggest that the drop in pore water pressure with the increasing flow rate was caused by the conversion of the pressure energy into kinetic energy. Because the particles inside the cavity moved rapidly with the jet of water, as the flow rate was further increased the particles began to move faster, resulting in an increase in their kinetic energy.

Imminent failure can be determined by noting the flow rate at which the pore water pressure stops increasing with increasing flow rate.

3.3 Imminent Failure

Based on observations and analysis, the onset of the failure mechanism of the granular bed induced by lateral seepage flow can be simplified as shown in Fig. 8. The *PIV* analysis revealed that the failure commenced with the outward movements of the grains (i.e., horizontally and vertically upwards) in the active area of flow, above the defect, which can be simplified as a right-triangular prism. This prism of granular material moved on surface at about 63° to the horizontal.

A prediction of the pore water pressure at the onset of failure can be made by considering equilibrium conditions for this geometry. Failure will commence once the sum of the vertical seepage forces on the triangular prism of grains exceeds the sum of the grains' buoyant weights (see Fig. 8). The vertical seepage

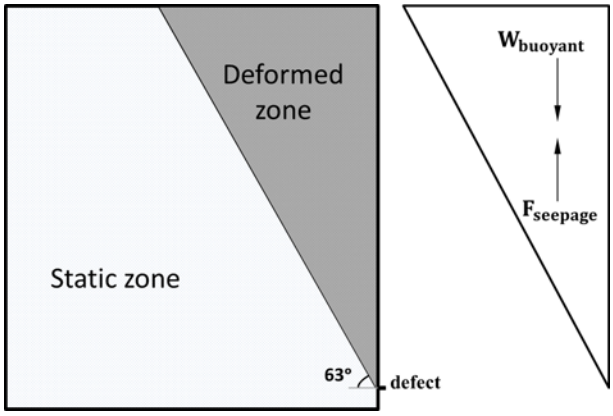

Fig. 8. A Method of Predicting Onset of Failure: (a) Observed Failure Geometry, (b) Free Body Diagram of the Body

force is provided by the jet of water, which can be related to either the water pressure at the base of the deformed bed (Alsaydalani and Clayton, 2014; Cui et al., 2014) or the inlet velocity (He et al., 2017).

Observations of the geometry of the deformed bed at the onset of failure indicated that the cross-sectional area of flow increased continuously from the bottom to the top (Fig. 8). Therefore, the area of the flow region increased with height, which caused the velocity to decrease.

This observed triangular flow geometry represents flow from a point source (i.e., flow from the defect located at the bottom of the bed to the side of the impermeable wall) that spread readily. The discharge velocity was higher near the defect but decreased sharply as the jet penetrated further into the granular material. It is anticipated that the non-Darcy effect would be more significant in the area near the defect because of the interaction of soil particles with the defect, turbulent flow in the soil and the changing geometry of the unconfined flow regime (van Zyl and Clayton, 2007; Alsaydalani and Clayton, 2014). Assuming a rate of flow of 350 l/h as observed in these tests and a cross-sectional area of flow in the vicinity of the defect 10 mm × 103 mm gives a Reynolds number (Re) of 86 (higher than the range, between 1 and 10, at which flow changes from laminar to turbulent flow), indicating that the flow in this region was a non-Darcy flow.

Ergun (1952) studied the nonlinear relationship between pressure drop and fluid velocity. He examined this phenomenon using a column, similar to that of Darcy, filled with granular materials, and allowed fluid to flow through the bed. Ergun (1952) examined its dependence on flow rate, size and shape of the particle, the porosity of the bed and fluid properties. Based on this study, Ergun developed an equation by equating the fluid energy loss to the sum of viscous energy and kinetic energy losses, giving the pressure loss per length of a packed bed:

$$\frac{\Delta P}{L} = A\frac{\mu}{\phi_s^2 d_p^2}\cdot\frac{(1-\varepsilon)^2}{\varepsilon^3}U + B\frac{\rho_f}{\phi_s d_p}\cdot\frac{(1-\varepsilon)}{\varepsilon^3}U^2 \quad (1)$$

Where,

A_c = Cross-sectional area of flow
d_p = Particle diameter
U = Superficial fluid velocity defined by $U = Q/A_c$, where Q is total flow rate through a cross section of area
ε = Porosity
μ = Fluid dynamic viscosity
ρ_f = Fluid density
ϕ_s = Particle shape factor

and A and B are constants determined by Ergun equal to 150 and 1.75, respectively.

Therefore, the Ergun equation, which takes into account the effect of viscous energy losses due to laminar flow and kinetic energy losses due to turbulent flow in the bed, is more appropriate in this case. Peng and Fan (1997) applied Ergun Eq. (1) and developed solutions for tapered fluidised beds using the gradient in the pressure drop. Details of mathematical derivations of the equations are presented in Peng and Fan (1997).

Observations such as those shown in Fig. 8 suggest that if the solutions of Peng and Fan (1997) were modified to account for the observed flow geometry (i.e., a right-triangular prism), they could be used to predict the pore pressure at the onset of failure.

The pressure at which failure starts can be determined from the calculations of vertical equilibrium for this geometry (i.e., a right-triangular prism) (see Fig. 8). Fig. 8(b) shows the free body diagram that is being evaluated, showing the upward vertical seepage force $F_{seepage}$ on the triangular prism of grains and the grains' buoyant weight $W_{buoyant}$, which exerts downward pressure. Considering the vertical equilibrium of the free body, failure occurs when the sum of the vertical seepage forces on the triangular prism of grains exceeds the sum of the grains' buoyant weight. On this basis, and adopting the solutions of Peng and Fan (1997), noted above, to account for the observed geometry (i.e., a right-triangular prism), pore pressures at the base of the deformed bed (i.e., at the defect) were predicted.

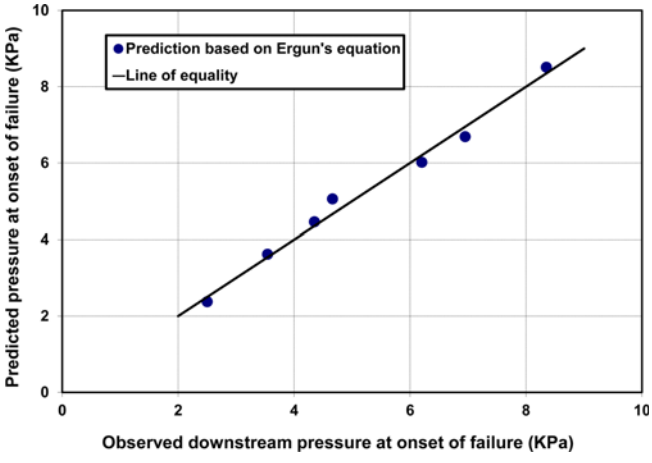

Fig. 9. Comparison between Observed and Predicted Downstream Pressures at the Onset of Failure Induced by Horizontal-Facing Flow

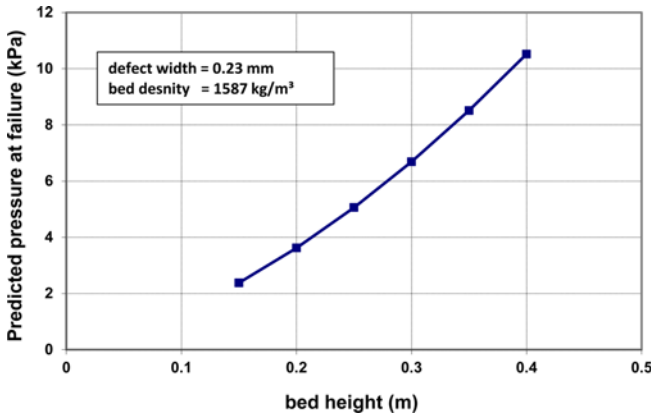

Fig. 10. Predicted Downstream Pressures at the Onset of Failure beside Horizontally Aligned Defects, as a Function of Bed Thickness

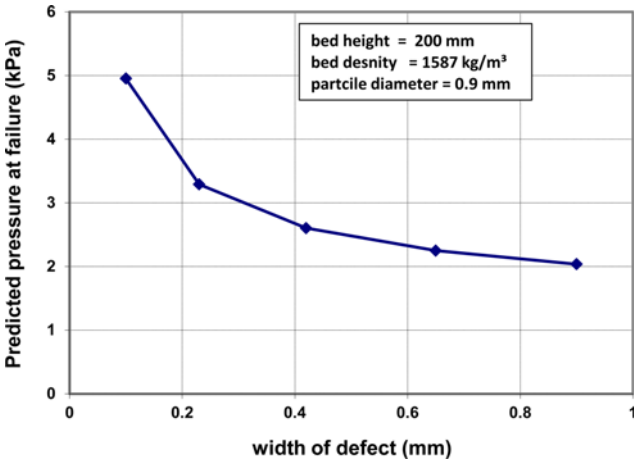

Fig. 11. Predicted Downstream Pressures at the Onset of Failure beside Horizontally Aligned Defects, as a Function of Defect Width

Figure 9 shows a comparison of the predicted pore pressures at the onset of failure obtained using the model with those measured in the current experiments; good agreement was obtained, as demonstrated in the line of equality in Fig. 9.

3.4 Effect of Bed Height

The values predicted using the Ergun equation (see Fig. 9) provide good estimates of the maximum pore water pressure at the onset of failure, giving confidence in this method. On this basis, predictions of the pressures at the onset of failure as a function of bed thickness were determined and plotted in Fig. 10. It can be observed that the higher the bed depth, the larger the pore water pressure downstream of the defect required to initiate failure because of the higher overburden pressure. Increasing the bed depth increases the effective stress of the bedding materials and hence the stability of the granular bed.

The data also show that the pore pressure increases nonlinearly with the burial depth (see Fig. 10). As noted, flow through defects in a structure does not adhere to Darcy's law, particularly at higher rates, at which failure may occur, because of the interaction of the soil particles with the defect, the turbulent flow in the soil and the changing geometry of the unconfined flow regime (van Zyl and Clayton, 2007; Alsaydalani and Clayton, 2014). Calculations of Re in the vicinity of the defect gave a high value of Re ~ 86 (see Section 3.3), which is higher than the range (between 1 and 10), at which flow changes from laminar to turbulent flow, indicating that flow in this region is non-Darcy flow.

3.5 Effect of Defect Size

The effect of defect size on the onset of failure of the granular bed is shown in Fig. 11 for five different defect sizes: 0.15, 0.23, 0.42, 0.65 and 0.90 mm. It can be observed that the smaller the defect size, the larger the pressure downstream of the defect required to initiate failure. It is predicted that downstream pressure and flow rate control the onset of failure. This is in agreement with Weisman and Lennon's (1994) observations for coastal fluidiser systems. It suggests that smaller defect openings require high pressure to produce sufficient flow rates to fluidise the bed of material.

For a more general case, the pressure required to displace particles away from the defect will depend on the in-situ effective stress level at the defect and the strength of the particulate material at that level.

3.6 Development of the Cavity Zone with Increasing Flow Rate

For an upward-facing water jet into a granular bed, He et al. (2017) observed that a sand bed underwent different phases with increasing flow rate: no cavity, a stable cavity above the jet, unstable cavity and full fluidisation. The cavity zone expanded progressively upward from the opening in the vertical direction as the flow rate increased until eventually it daylighted at the bed surface and formed an open fluidised zone. This finding is consistent with the observations of Alsaydalani and Clayton (2014) for the mechanisms of fluidisation in granular soils.

For a downward-facing jet (i.e., a downwardly directed vertical water jet), Niven and Khalili (1998) presented schematic diagrams of the scouring of granular material. Their observations revealed an initial stage of sand-bed erosion that was followed by a stable, open, fluidised zone. With increasing jet depth, the fluidised zones became unstable while circulating around the jet. Ultimately, the cavity closed above the fluidised zone (submerged fluidised cavity), which could not be observed at the bed surface.

For horizontally facing water jets, such as those resulting from a vertical and impermeable surface such as a defected retaining wall or a crack in the core of an earthen dam, observations made in this study using *PIV* revealed that cavity formation is associated with a displacement (deformation) of the grains in the active area of flow. The particles were forced outwards (horizontally and vertically upwards) and a cavity began to develop in front of the defect as the flow rate approached the point at the onset of failure. This deformation created a space for a cavity to form in

the vicinity of the defect. The geometry of deformation observed in this study with a horizontally placed water jet (i.e., a right-triangular prism; see Fig. 8) differs from that induced by an upwardly oriented vertical water jet (Alsaydalani and Clayton, 2014). Alsaydalani and Clayton (2014) noted a geometry of deformation resembling a tapered block. Their finding can be attributed to the orientation of the jet; similar deformation was not observed in this study. As the flow rate was increased further, the cavity enlarged. This enlargement occurred horizontally in the direction of the jet. However, as this zone expanded away from the defect, it gradually propagated upwards to the bed surface. Eventually, the cavity zone broke through to the surface of the bed.

4. Conclusions

Failure by seepage is considered to cause the most serious accidents in civil engineering. Such failures can occur in multiple settings, including interlocking sheet piles, earth dams and fractured underground pipes that lead to cavities and sinkholes.

This study investigated the failure mechanism of a granular bed subjected to lateral seepage flow using the *PIV* technique. The experiments revealed several stages of failure during repeated experiments. Failure occurs in the following sequence under a controlled and increasing flow rate:

1. At a sufficiently low flow rate, the bed remains motionless and acts as a stable bed.
2. At sufficiently large Q values, the bed becomes deformed and the granular soil moves away from the defect opening (the grains move horizontally and vertically upwards in the active area of the bed). This deformation creates a space for a cavity to form in the vicinity of the defect. The grains inside the cavity move rapidly with the jet and grains outside the cavity remained fixed in the bed. The *PIV* analyses showed the movement of grains and boundaries between regions in which sand grains either did or did not move.
3. With increasing flow rate, the cavity zone expands. This expansion primarily occurs horizontally in the direction of the jet. However, as this zone expands away from the defect it gradually propagates upwards to the bed surface.
4. Finally, the cavity zone breaks through to the bed surface at high flow rates.

For a horizontally facing water jet, the onset of failure is modulated by the rate of the flow and the pore water pressure immediately downstream of the defect. The smaller the defect size, the larger the pore water pressure at the defect opening required to initiate failure. This finding can be attributed to small defect openings requiring high upstream and downstream pressure to discharge a sufficient amount of fluid to overcome the effective weight of the granular bed. Increasing the bed depth increases the effective stress of the bedding materials and hence the stability of the granular bed.

This study provides valuable insights into the failure mechanism of granular materials triggered by lateral seepage flow.

Acknowledgements

The author thanks the civil engineering department at Umm Al-Qura University, where the experimental work was carried out. Part of this acknowledgement goes to Dr Eltohamy for his valuable comments and discussion and to Eng. Sahito for all his help and assistance in the lab.

Nomenclature

A in Eq. (1) = Constants, determined by Ergun (1952), equal to 150
B in Eq. (1) = Constants, determined by Ergun (1952), equal to 1.75
A_c = Cross-sectional area of flow
d_p = Particle diameter
Q = Flow rate through a cross section of area, A_c
Re = Reynolds number
U = Fluid velocity ($U = Q / A_c$)
V = Average velocity of flow (flow per unit cross section of soil)
v = Kinematic viscosity of the fluid
ε = Porosity
μ = Dynamic viscosity of fluid
ρ_f = Fluid density
ρ_s = Solids density
ϕ_s = Sphericity

ORCID

Majed Omar Alsaydalani https://orcid.org/0000-0002-1058-6215

References

Adrian RJ (1991) Particle image techniques for experimental fluid mechanics. *Annual Review of Fluid Mechanics* 23(1):261-304, DOI: 10.1146/annurev.fl.23.010191.001401

Al-Karni A (2000) Stability of saturated cohesionless soil layer due to water flowing from a broken underground pipeline. *Journal of King Saud University, Engineering Science* 12(1):27-44, DOI: 10.1016/S1018-3639(18)30705-0

Allersma HG, Plenevaux F, Wintgens J (2003) Centrifuge research on suction piles: Installation and bearing capacity. Proceedings of BGA international conference on foundations: Innovations, observations, design and practice, September 2-5, Dundee, UK

Alsaydalani MOA, Clayton CRI (2014) Internal fluidization in granular soils. *Journal of Geotechnical and Geoenvironmental Engineering* 140(3):04013024-1–04013024-10, DOI: 10.1061/(ASCE)GT.1943-5606.0001039

Cui X, Li J, Chan A, Chapman D (2014) Coupled DEM–LBM simulation of internal fluidisation induced by a leaking pipe. *Powder Technology* 254:299-306, DOI: 10.1016/j.powtec.2014.01.048

Ergun S (1952) Fluid flow through packed columns. *Journal of Chemical Engineering Progress* 48(2):89-94

Harireche O, Mehravar M, Alani AM (2014) Soil conditions and bounds to suction during the installation of caisson foundations in sand. *Ocean Engineering* 88:164-173, DOI: 10.1016/j.oceaneng.2014.06.033

Harr ME (1962) Groundwater and seepage. McGraw Hill, New York, NY, USA

He Y, Zhu DZ, Zhang T, Shao Y, Yu T (2017) Experimental observations on the initiation of sand-bed erosion by an upward water jet. *Journal of Hydraulic Engineering* 143(7):06017007, DOI: 10.1061/(ASCE)HY.1943-7900.0001302

Keane RD, Adrian RJ (1992) Theory of cross-correlation analysis of PIV images. *Applied Scientific Research* 49(3):191-215, DOI: 10.1007/BF00384623

Kjaernsli B, Torblaa I (1968) Leakage through horizontal cracks in the core of Hyttejuvet Dam. No. 80:39-47, Norwegian Geotechnical Institute Publication, Oslo, Norway

Niven RK (2002) Physical insight into the Ergun and Wen & Yu equations for fluid flow in packed and fluidised beds. *Chemical Engineering Science* 57(3):527-534, DOI: 10.1016/S0009-2509(01)00371-2

Niven RK, Khalili N (1998) In situ fluidization by a single internal vertical jet. *Journal of Hydraulic Research* 36(2):199-228, DOI: 10.1080/00221689809498633

Omofunmi OE, Kolo JG, Oladipo AS, Diabana PD, Ojo AS (2017) A review on effects and control of seepage through earth-fill dam. *Current Journal of Applied Science and Technology* 22(5):1-11, DOI: 10.9734/CJAST/2017/28538

Peng Y, Fan L (1997) Hydrodynamics characteristics of fluidization in liquid/solid taper beds. *Chemical Engineering Science* 52(14):2277-2290, DOI: 10.1016/S0009-2509(97)00061-4

Pillai VS, Muhunthan B, Sasiharan N (2004) The failure of Teton Dam — A new theory based on state based soil mechanics. Proceedings of the fifth international conference on case histories in geotechnical engineering, April 14-17, New York, NY, USA

Rice JD, Duncan M (2010) Findings of case histories on the long-term performance of seepage barriers in dams. *Journal of Geotechnical and Geoenvironmental Engineering* 136(1):2-35, DOI: 10.1061/(ASCE)GT.1943-5606.0000175

Richards S, Reddy K (2007) Critical appraisal of piping phenomena in earth dams. *Bulletin of Engineering Geology and the Environment* 66(4):381-402, DOI: 10.1007/s10064-007-0095-0

Sveen JK (2004) An introduction to MatPIV v. 1.6.1. University of Oslo, Oslo, Norway

Terzaghi K (1939) Soil mechanics: A new chapter in engineering science. *Institution of Civil Engineers* 12(1039):106-141, DOI: 10.1038/143865a0

Tran MN, Randolph MF, Airey DW (2004) Experimental study of suction installation of caissons in dense sand. Proceedings of the 23rd international conference on offshore mechanics and arctic engineering, June 20-25,Vancouver, Canada, DOI: 10.1115/OMAE2004-51076

Tran MN, Randolph MF, Airey DW (2005) Study of sand heave formation in suction caissons using particle image velocimetry (PIV). Proceedings of the 1st international symposium on frontiers in offshore geotechnics, September 19-21, Perth, Australia

van Zyl JE, Alsaydalani MOA, Clayton CRI, Bird T, Dennis A (2013) Soil fluidisation outside leaks in water distribution pipes — Preliminary observations. *Proceedings of the ICE — Water Management* 166(10):546-555, DOI: 10.1680/wama.11.00119

van Zyl JE, Clayton CRI (2007) The effect of pressure on leakage in water distribution systems. *Proceedings of the Institution of Civil Engineers — Water Management* 160(2):109-114, DOI: 10.1680/wama.2007.160.2.109

Walski T, Bezts W, Posluzny E, Weir M, Whitman B (2006) Modelling leakage reduction through pressure control. *Journal of the American Water Work Association* 98(4):147-152, DOI: 10.1002/j.1551-8833.2006.tb07642.x

Weisman RN, Lennon GP (1994) Design of fluidiser systems for coastal engineering. *Journal of Waterway, Port, Coastal, and Ocean Engineering* 120(5):468-487, DOI: 10.1061/(ASCE)0733-950X(1994)120:5(468)

Zoueshtiagh F, Merlen A (2007) Effect of a vertically flowing water jet underneath a granular bed. *Physical Review E* 75(5):056313-1-1056313-12, DOI: 10.1103/PhysRevE.75.056313